Diffusion-Weighted Magnetic Resonance Imaging of Focal Hepatic Nodules in an Experimental Hepatocellular Carcinoma Rat Model[1]

Hui Xu, PhD,* Xuan Li, MD,* Jing-Xia Xie, MD, Zheng-Han Yang, MD, Bin Wang, MD

Rationale and Objectives. We sought to investigate the value of diffusion-weighted MR imaging in evaluating focal hepatic nodules in an experimental hepatocellular carcinoma (HCC) rat model.

Materials and Methods. Forty rats with chemically induced primary hepatic nodules ranging pathologically from regenerative nodules (RNs) to dysplastic nodules (DNs) to HCC were examined with diffusion-weighted imaging. The apparent diffusion coefficient (ADC) values of hepatic nodular lesions were calculated. Tukey's HSD post hoc test was used to compare the difference in ADC values between different hepatic nodular lesions.

Results. Eight RNs, 16 DNs, 7 well-differentiated HCCs (HCC_{well}), 11 moderately differentiated HCCs (HCC_{mod}), and 14 poorly differentiated HCCs (HCC_{poor}) were evaluated. There was no significant difference between RNs and DNs ($P > 0.05$). Although the ADC values of HCC_{well} were slightly lower than those of DNs, there was no significant difference between them ($P > 0.05$). The ADC values of HCC_{mod} and HCC_{poor} were significantly higher ($P < 0.05$) than those of other nodules, and no significant difference was seen between HCC_{mod} and HCC_{poor} ($P > 0.05$).

Conclusion. Diffusion-weighted magnetic resonance imaging can be useful in characterizing focal hepatic nodular lesions, but ADC values cannot be used efficiently to distinguish HCC_{well} from DNs.

Key words. Magnetic resonance imaging; diffusion; hepatocellular carcinoma; dysplastic nodules

Hepatocellular carcinoma (HCC) is the most common primary malignant tumor of the liver, with highest incidences occurring in Africa, Southeast Asia, and China (1–3). A cirrhotic liver is often the background from which HCC arises. One pathway to the development of HCC in patients with cirrhosis is a multistep carcinogenesis process from benign regenerative nodule (RN) to dysplastic nodule (DN) to a dysplastic nodule with microscopic foci of HCC, which may enlarge and replace the nodule giving rise to a small HCC, and finally to the overt HCC (4–7). DNs are considered precancerous lesions of HCC (8, 9). Therefore, it is clinically important to detect DNs and HCC at an early stage for prompt surgical resection, transplantation, or local ablation therapy to ensure a better chance of survival.

Diffusion-weighted (DW) MRI is an imaging technique used to show microscopic motion in biologic tissues (10, 11). The apparent diffusion coefficient (ADC), a quantity calculated from the DW MR images, combines the effects of capillary perfusion and water diffusion in the extracellular extravascular space (10, 11). Thus, DW MRI is currently the only imaging method for assessing

Acad Radiol 2007; 14:279–286

[1] From the Department of Radiology (origin of work), Peking University Third Hospital, 49 North Garden Road, Haidian District, Beijing, 100083 China (H.X., X.L., J.-X.X.); Department of Radiology, Beijing Hospital, Beijing, 100730 China (Z.-H.Y.); and Department of Radiology, the Affiliated Hospital, Weifang Medical University, Weifang, 261041 China (B.W.). Received October 18, 2006; accepted December 8, 2006. This work was supported by the Nature and Science Foundation of Beijing (No. 7063091). **Address correspondence to** J.-X.X. or Z.-H.Y.: e-mail: mrhepatic@yahoo.com.cn or zhenghanyang@263.net, respectively.

* Hui Xu, PhD, and Xuan Li, MD, contributed equally to this work.

doi:10.1016/j.acra.2006.12.005

in vivo perfusion and diffusion simultaneously within the same organ (10–12).

DW MRI has recently been used to characterize abdominal organs and hepatic lesions (13–16). Results of these studies showed principally that DW MRI, by means of ADC measurement, can be used to characterize focal hepatic lesions (13–16). Benign lesions, such as hepatic cysts and hemangiomas, showed higher ADCs than those of malignant lesions (HCC and metastases). To our knowledge, very few studies have reported the ADCs of RNs and DNs in cirrhotic liver.

The purpose of this study was to investigate the value of DW MRI in the evaluation of RNs, DNs, and HCC in an experimental rat model. This model was induced by diethylnitrosamine (DEN), which results in hepatic nodules with histological features similar to the type of lesions observed in human cirrhotic liver carcinogenesis (17–19).

MATERIALS AND METHODS

Animal Model

The experiment was performed in accordance with the *Guide for the Care and Use of Laboratory Animals* (National Institutes of Health publication No. 85-23, revised 1996), with the approval of the local ethical committee for animal care and use. Six-week-old male rats (n = 40) of the Sprague-Dawley strain, weighing 120−150 g, were supplied by the Department of Laboratory Animal Science, Peking University, Beijing, China. The animals were acclimated for 1 week and maintained under specific pathogen-free environmental conditions with lighting from 9:00 [scap]am[r] to 9:00 [scap]pm[r], temperature of 22 ± 2°C, and relative humidity of 45−60% and were fed chow pellets and solution ad libitum during the entire study period. HCC was induced with 70 mg/kg DEN (0.95 g/ml; Sigma Chemical Co., St. Louis, MO) intragastrically once a week for 10 weeks.

MR Imaging

From week 10 to week 20 after induction of HCC by DEN, three or four treated animals were randomly scanned every week. After fasting for 12 hours, each rat was anaesthetized with 40 mg/kg pentobarbital sodium (Nembutal; Beijing Chemical Co., Beijing, China) intraperitoneally before imaging.

The rats were examined with a 1.5-T whole-body MR system (Sonata; Siemens, Erlangen, Germany) with a maximum gradient capability of 40 mT/m. A two-channel phased-array coil (50 mm in diameter; Chen Guang Medical Science Co., Shanghai, China) specially designed for rats was used to obtain all MR images. The rats were placed in a supine position inside the coil with the liver region located in the center of the coil and the abdomen fixed with adhesive tape to reduce respiratory movement.

To detect the hepatic nodules, a conventional liver MRI protocol was used as follows: T2-weighted turbo spin-echo (TSE) transverse, sagittal, and coronal orientation sequences with fat saturation (TR = 3,000 ms, TE = 79 ms, a flip angle of 150°, echo train length of 7, field of view 90 mm × 65 mm, matrix 192 × 135, slice thickness 3 mm), transverse two-dimensional T1-weighted fast low-angle shot (FLASH) sequence with fat saturation (TR = 250 ms, TE = 3.53 ms, a flip angle of 70°, field of view 90 mm × 55 mm, matrix 192 × 135, slice thickness 3 mm).

Transverse diffusion-weighted multisection echo-planar MRI was performed with two groups of diffusion gradient b values: b = 0, 600 sec/mm^2 and b = 0, 1,000 sec/mm^2. In the sequence, a unidirectional diffusion gradient was applied along the section-select direction (z axis). The following parameters were used for this sequence: TR = 3,000 ms; TE = 79 ms (b = 0, 600 sec/mm^2) or TE = 88 ms (b = 0, 1,000 sec/mm^2); field of view 90 × 68 mm; matrix 64 × 64; section thickness 3 mm. Fat saturation was used to avoid chemical shift artifacts.

Histology

The animal was killed after completion of MRI. The liver was removed and cut sequentially into 3-mm sections in the transverse plane that corresponded as closely as possible to the MRI plane. We identified the nodule that corresponded to DW MRI; then the tissue was fixed in 4% buffered formalin and embedded in paraffin, and thinner sections of 5 μm were cut and stained with hematoxylin-eosin for histological examination. Histological examination was conducted by two experienced hepatopathologists. By using the diagnostic criteria from the International Working Party's *Terminology of Nodular Hepatocellular Lesions* (4), nodules were classified as RN, DN, well-differentiated HCC (HCC_{well}), moderately differentiated HCC (HCC_{mod}), and poorly differentiated HCC (HCC_{poor}).

Image Analysis

Quantitative ADC maps were calculated automatically on a voxel-by-voxel basis with the MR system. The ADC

was calculated with a linear regression analysis of the function $S = S_0 \cdot \exp(-b \times \text{ADC})$, where b is the diffusion factor (600 sec/mm^2 or 1,000 sec/mm^2), S is the signal intensity after application of the diffusion gradient, and S_0 is the signal intensity at $b = 0$ sec/mm^2. ADC of the liver lesions calculated with two sets of b values, one set was 0 and 600 sec/mm^2 (the low one), another set was 0 and 1000 sec/mm^2 (the high one).

The conventional MRI protocol could distinguish the hepatic nodular lesions clearly. A circular region of interest (ROI) was drawn to encompass as much of the nodular lesion as possible in the transverse ADC maps. To ensure that the same areas were measured, the ROIs were copied and pasted onto the T1, T2, and DW MR images and ADC maps. For cirrhotic liver, ROIs were always placed in the posterior segment of the right hepatic lobe to avoid artifacts from large vessels, ADC values of cirrhotic liver were measured in two consecutive planes of ADC maps separately, and the measurements were averaged.

Statistical Analysis

Data were first evaluated using one-way analysis of variance (ANOVA), and then Tukey's HSD post hoc test was used to compare the difference in ADC values between cirrhotic liver, RN, DN, HCC_{well}, HCC_{mod}, and HCC_{poor} using statistical software (SPSS for Windows, Beijing, ersion 12; SPSS Inc, Chicago, IL). A two-tailed P-value of less than .05 was required for statistical significance.

RESULTS

Among 56 nodules (with diameters between 3 mm and 17 mm) revealed by MRI and precisely corresponding with the pathology, we identified 8 cases of RN, 16 of DN, 7 of HCC_{well}, 11 of HCC_{mod}, and 14 of HCC_{poor}. The ADC values of cirrhotic liver, RN, DN, HCC_{well}, HCC_{mod}, and HCC_{poor} calculated with various sets of b values are shown in Table 1. The mean ADC values for the cirrhotic liver and nodular lesions tended to be smaller when the maximum b value used was greater (Fig. 1).

There was no significant difference among the cirrhotic liver, RN, and DN. Although the ADC value of HCC_{well} (Fig. 2) was slightly lower than that of DN (Fig. 4), there was no significant difference between them. The ADC values of HCC_{mod} (Fig. 3) and HCC_{poor} (Fig. 4) were significantly higher than for other hepatic nodules, and no significant difference was seen between the ADC values of HCC_{mod} and HCC_{poor}.

Table 1
ADC values of liver lesions calculated with various sets of *b* values

Liver lesions	No.	ADC ($\times 10^{-3}$ mm^2/sec) of liver lesions calculated with various sets of b values: Low b values (b = 0, 600 sec/mm^2)	High b values (b = 0, 1,000 sec/mm^2)
Cirrhotic liver	32	1.08 ± 0.09	0.94 ± 0.09
RNs	8	1.01 ± 0.13	0.90 ± 0.10
DNs	16	1.02 ± 0.11	0.91 ± 0.11
HCC_{well}	7	0.98 ± 0.17	0.84 ± 0.12
HCC_{mod}	11	1.21 ± 0.17	1.08 ± 0.14
HCC_{poor}	14	1.24 ± 0.21	1.11 ± 0.18

Data are expressed as mean ± SD. RN, regenerative nodule; DN, dysplastic nodule; HCC_{well}, well-differentiated HCC; HCC_{mod}, moderately differentiated HCC; HCC_{poor}, poorly differentiated HCC.

DISCUSSION

In our study, we explored the ADC values of benign HCC nodules, including cases of RNs and DNs. The ADC values of benign HCC nodules were slightly smaller than those of adjacent cirrhotic liver parenchyma, and some overlaps occurred of the ADC values. Histologically, RNs develop as a part of the repair process following hepatocyte injury; they comprise a local proliferation of hepatocytes surrounded by fibrous septa, and the hepatocytes inside the nodules are similar to those of neighboring cirrhotic liver (4, 8, 20). As for DNs, they are regenerative nodules that contain atypical cells without definite histological features of malignancy, and they have slightly higher cellular density than that of cirrhotic liver (4, 8, 20). Therefore, it is not surprising that we did not obtain a significant difference in ADC values between the benign hepatic cirrhotic nodules and cirrhotic liver.

Along the pathway from DN to HCC_{well}, the tumor cell density and the nucleocytoplasmic ratio increase to some degree (4). In our study, although the ADC values of some HCC_{well} were lower than for DNs, there was no statistically significant difference between them. Considering that there was an overlap in the distribution of ADC values between HCC_{well} and DNs and it is still difficult to distinguish them histologically (20), this finding was reasonable. Another explanation is that the speed of hepatocarcinogenesis was very fast in this model and produced a continuous spectrum of abnormality, resulting in overlap-

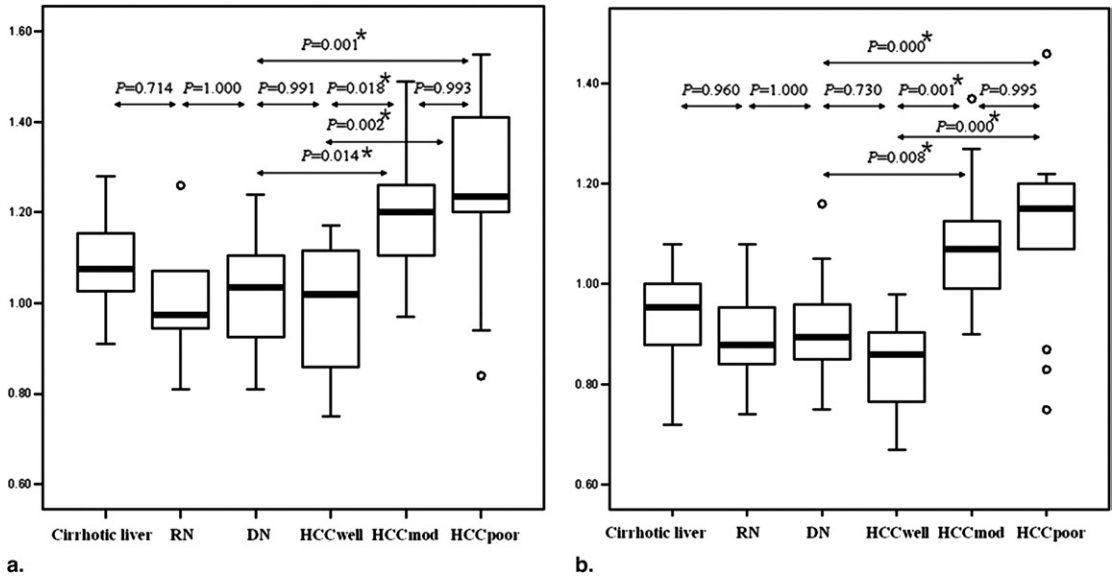

Figure 1. The ADC values of liver lesions calculated with $b = 0$, 600 sec/mm^2 (**A**) and $b = 0$, 1,000 sec/mm^2(**B**). There was no significant difference among the cirrhotic liver, RNs, and DNs. Although the ADC value of HCC_{well} was slightly lower than that of DNs, there was no significant difference between them. The ADC values of HCC_{mod} and HCC_{poor} were significantly higher than other hepatic nodules and no significant difference was seen between them. *$P < .05$. RN, regenerative nodules; DN, dysplastic nodules; HCC_{well}, well-differentiated HCC; HCC_{mod}, moderately differentiated HCC; HCC_{poor}, poorly differentiated HCC.

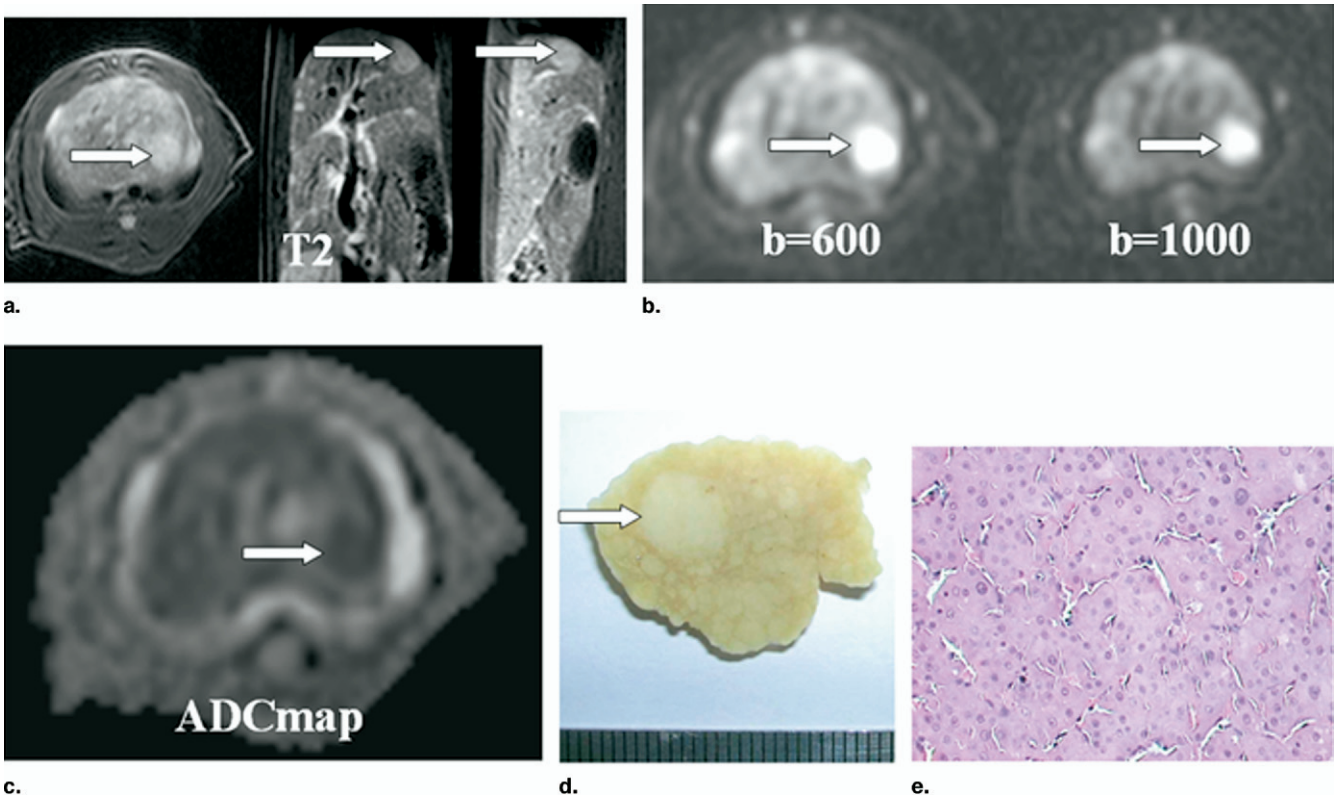

Figure 2. Well-differentiated HCC. (**A**) Transverse, coronal, and sagittal turbo spin-echo fat-saturated T2-weighted MR image shows a hyperintense tumor (*white arrow*). The tumor is hyperintense on DW MR images ($b = 600$ sec/mm^2, $b = 1{,}000$ sec/mm^2) (**B**) and hypointense on ADC map (calculated with $b = 0$, 1,000 sec/mm^2) (**C**). (**D**) Resected specimen of the tumor (*white arrow*). (**E**) Histologic examination results revealed a well-differentiated HCC. (Hematoxylin-eosin stain; original magnification, ×400.)

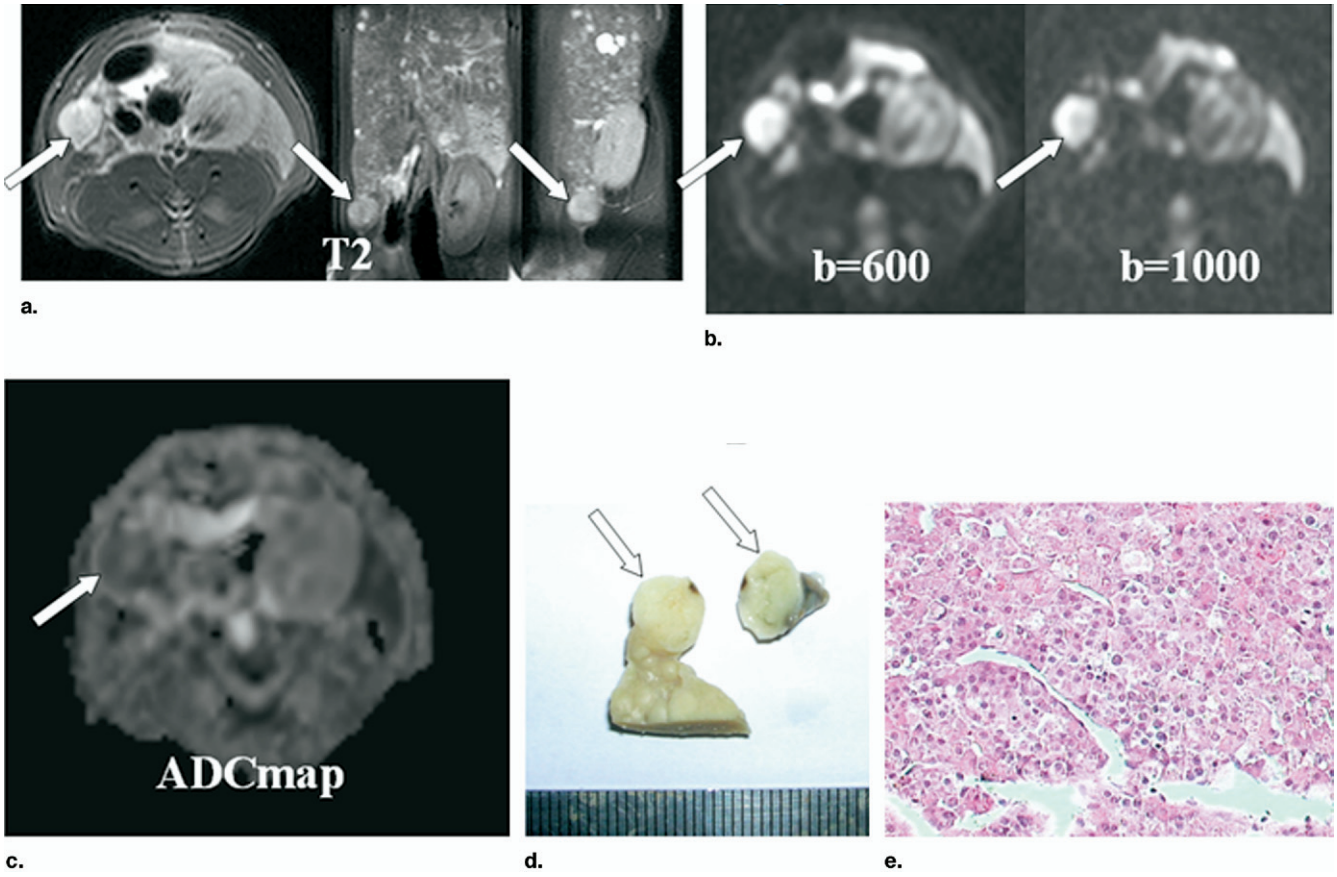

Figure 3. Moderately differentiated HCC. (**A**) Transverse, coronal, and sagittal turbo spin-echo fat-saturated T2-weighted MR image shows a hyperintense nodule (*white arrow*) prominent in the liver. (**B**) The nodular lesion is hyperintense on DW MR images (b = 600 sec/mm^2, b = 1,000 sec/mm^2). (**C**) On the ADC map (calculated with b = 0, 1,000 sec/mm^2), the nodular lesion is slightly hypointense. (**D**) Corresponding transverse sections from the liver depict the nodule (*white arrow*). (**E**) The nodule was histologically proved to be moderately differentiated HCC. (Hematoxylin-eosin stain; original magnification, ×400.)

ping histological characteristics in these two kinds of nodules and preventing a statistically significant difference between them. In addition, another reason for this finding may be the relatively small sample of HCC_{well} and DNs in our study. Therefore, based on our data, ADC values cannot be used efficiently to distinguish HCC_{well} from DNs. Accompanying the malignant evolution from DNs to HCC, there is a gradual change in blood supply from portal to arterial (9, 21). These changes in intranodular blood could be potentially measured with perfusion-weighted MRI (22). Therefore, if ADC values could not characterize liver lesions, perfusion-weighted MRI would provide complementary data to DW MRI differentiation of lesion type.

In our study, HCC nodules occurred 15 weeks after induction by DEN and seemed to be markedly developed after 16 weeks. Both necrosis and hemorrhage were common in HCC_{mod} and HCC_{poor} (Fig. 4). Most HCC_{mod} and HCC_{poor} had higher ADC values than DNs. This may be because we measured ADC values by placing a region of interest over the entire area of the HCC nodules, and we could not precisely distinguish the areas of necrosis and hemorrhage from viable tissue in HCC; a contamination error therefore could not be avoided. Furthermore, based on our data, the increase of ADC values appears to have a trend based on the severity of the lesion. An explanation for this is that as the lesion progresses, extracellular water tends to be greater, intratumoral hemorrhage and accompanying tumor necrosis are more likely to take place, and the ADC values of the lesion increase. This could be used as an adjuvant parameter in diagnosis, and additional studies are necessary in the future.

When tumor cells are alive, their membranes are intact and can restrict the movement or diffusion of water molecules (23). Conversely, when the cells are dead, their membranes are broken down and can no longer restrict

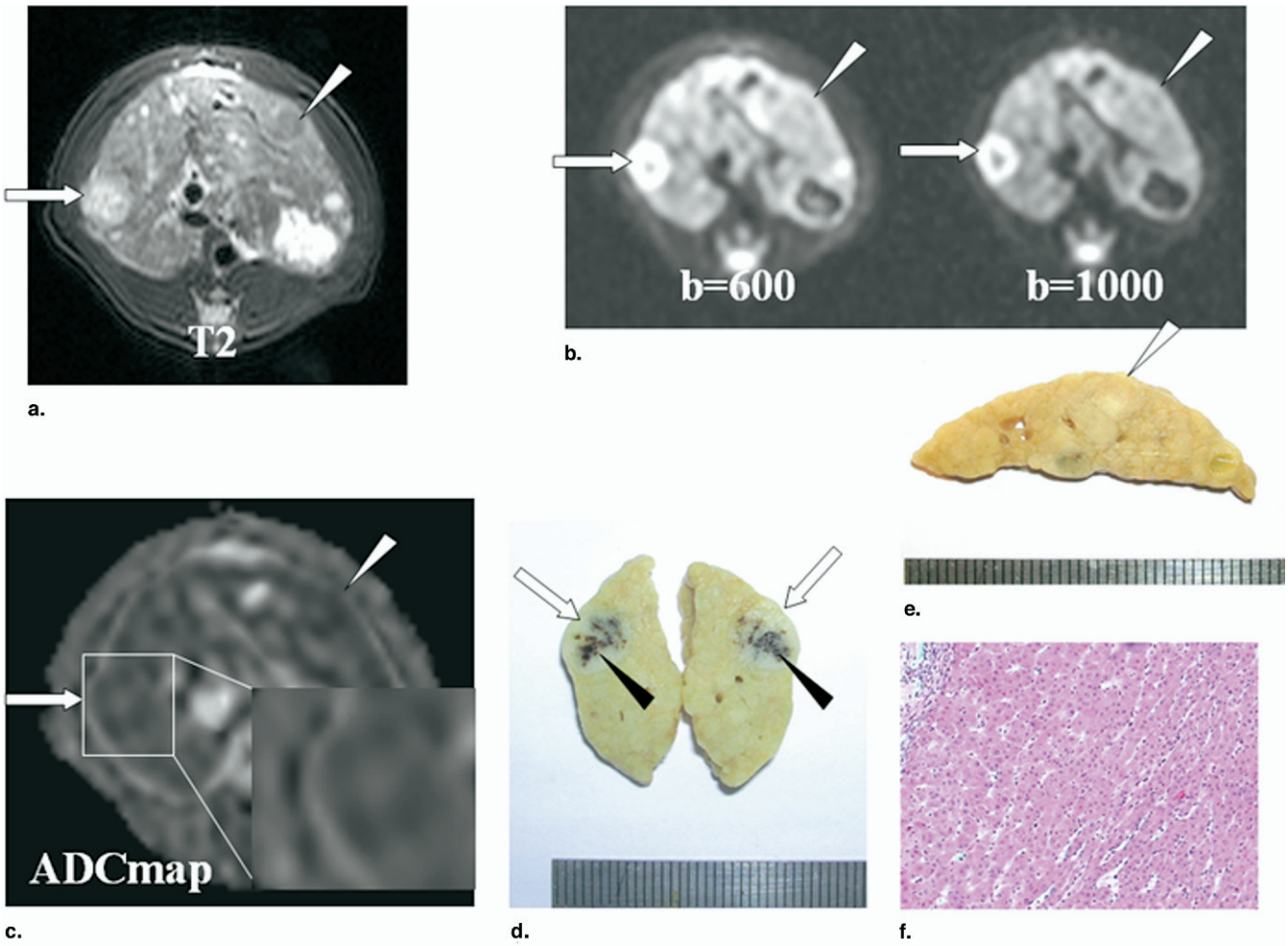

Figure 4. Poorly differentiated HCC and dysplastic nodule. (**A**) Transverse turbo spin-echo fat-saturated T2-weighted MR image shows the poorly differentiated HCC (*white arrow*) appears as a heterogeneous rounded area of hyperintensity located in the right lobe of the liver, and the DN (*white arrowhead*) appears as a hypointensity nodule in the left. (**B**) On DW MR images (b = 600 sec/mm^2, b = 1,000 sec/mm^2), a rim of high signal intensity representing viable tumor cells is clearly seen in the tumor (*white arrow*), reflecting intact cell membranes and restriction of water molecules. The area of necrosis at the central core of the tumor is identified as a black zone, reflecting increased diffusion of water molecules caused by breakdown of cell membranes. (**C**) On an ADC map (calculated with b = 0, 1,000 sec/mm^2), the area of tumor necrosis is a bright zone and a rim of low signal intensity representing the viable tumor is clearly seen. The DN (*white arrowhead*) appears isointense to the adjacent liver parenchyma on DW MR images and the ADC map. (**D**) Resected specimen reveals a nodular lesion (*white arrow*) about 5 mm in diameter containing darker areas (*black arrowhead*). At microscopic examination (not shown), the whole lesion was verified to be poorly differentiated HCC, while the darker area in it was necrotic. (**E**) Corresponding transverse sections from the liver depict the nodule (*white arrowhead*). (**F**) Histologic examination revealed the DN. (Hematoxylin-eosin stain; original magnification, ×200.)

diffusion of water molecules. Many researchers have reported that necrotic tissue of tumors shows high ADC values (23–27). This higher diffusion rate can be explained by the presence of greater amounts of extracellular water within the necrotic region caused by the loss of cell membranes that can no longer compartmentalize water molecules (26, 28), which allows free diffusion to take place. It could also be attributed to shrinkage of apoptotic cells, which would result in an increase in the extracellular water fraction (29). Of course, high ADC values provide information on the microenvironment of the entire tumor and indicate the biological characteristics of HCC that easy to necrosis and hemorrhage. According to these characteristics, we can distinguish the HCC_{mod} and HCC_{poor} from benign hepatic cirrhotic nodules.

ADC values calculated on the basis of higher b values reduce the influence of perfusion and approximate true diffusion. But with the increase of b values, the quality of a DW image is greatly diminished and the signal-to-noise ratio tends to decline because the T2 relaxation time of

liver tissue is short. Therefore, finding an appropriate *b* value for liver tissue is very important. In this study, high *b* values ($b = 600$ sec/mm^2, $b = 1{,}000$ sec/mm^2) were used and the image quality at $b = 600$ sec/mm^2 was better than at $b = 1{,}000$ sec/mm^2. Therefore, we consider that *b* values smaller than 1,000 sec/mm^2 would be appropriate for liver in a 1.5-T MR scanner.

In this study, because lack of high-field MR scanner, we used a customized rat coil to acquire MR images from the rats and we obtained satisfactory results. Therefore, for those institutions that do not have a dedicated high-field small animal MR scanner, this could be a useful approach. It could be translated from animals to human patients.

A potential shortcoming of this study is that there was an anatomic distortion present in the DW MRI and ADC maps when $b = 1{,}000$ sec/mm^2 was used. New imaging sequences and high-field-strength 3.0-T imagers would improve image quality and may be useful in future investigations. Second, the sample of HCC_{well} nodules was relatively small; further studies with a larger number of nodules are needed in the future. Third, the animal model used is a short-term model induced by DEN, and it cannot absolutely recapitulate the progression of carcinogenesis in humans. Although there are significant differences between HCC and benign tumors in the study, the results cannot be extrapolated to human use immediately. For DW MRI to be clinically feasible and reliable in the future, further efforts to screen hepatic nodules in HCC high-risk populations are still essential. Finally, motion artifacts due to cardiac and respiratory motions would affect the DW MRI. Both ECG-gated techniques and respiration-gated methods would be useful to reduce motion artifacts. In this study, none of the two gating methods were used. For the ECG gating, because the heart rate of the rat was so fast (about 400 counts per minute), we could not perform ECG gating. To reduce the impact of respiratory movement, we apply two methods. First, we use pentobarbital sodium (Nembutal) to induce anesthesia, which can inhibit the respiration of rats in some degree, and we use an appropriately deep anesthesia to control the respiration movements of rats. Second, the rat is placed supine inside the coil with the liver region located in the center of the coil and the abdomen of the rat fixed with adhesive tape to control respirations. With use of the two methods, the respiration movements of rats were controlled effectively. In addition, the customized rat coil we used could significantly improve the image quality, so we obtained satisfactory results without the ECG-gating and respiration-gating methods used during the DW MR image acquisitions. Of course, for clinical use of DW MRI in patients, ECG-gating or respiration-gating methods should be necessary.

In conclusion, DW MRI can provide additional information for the characterization of hepatic lesions and is potentially useful for differentiating between benign and malignant hepatic nodules. However, we currently cannot distinguish HCC_{well} from DNs by depending only on ADC values.

ACKNOWLEDGMENTS

We gratefully acknowledge the assistance of Professor Zhuo-Zhao Zheng for MR technical support and thank Professor Zheng Wang and Mrs. Xue-Hui Yao for their invaluable help.

REFERENCES

1. Unoura M, Kaneko S, Matsushita E, et al. High-risk groups and screening strategies for early detection of hepatocellular carcinoma in patients with chronic liver disease. Hepatogastroenterology 1993; 40:305–310.
2. Parkin DM. Global cancer statistics in the year 2000. Lancet Oncol 2001; 2:533–543.
3. Bosch FX, Ribes J, Borras J. Epidemiology of primary liver cancer. Semin Liver Dis 1999; 19:271–285.
4. International Working Party. Terminology of nodular hepatocellular lesions. Hepatology 1995; 22:983–993.
5. Kobayashi M, Ikeda K, Hosaka T, et al. Dysplastic nodules frequently develop into hepatocellular carcinoma in patients with chronic viral hepatitis and cirrhosis. Cancer 2006; 106:636–647.
6. Efremidis SC, Hytiroglou P. The multistep process of hepatocarcinogenesis in cirrhosis with imaging correlation. Eur Radiol 2002; 12:753–764.
7. Taguchi K, Aishima S, Matsuura S, et al. Significance of the relationship between irregular regeneration and two hepatocarcinogenic pathways: "De novo" and so-called "dysplastic nodule-hepatocellular carcinoma" sequence. J Surg Oncol 2005; 92:100–103.
8. Kojiro M. Focus on dysplastic nodules and early hepatocellular carcinoma: An Eastern point of view. Liver Transpl 2004; 10:S3–S8.
9. Hayashi M, Matsui O, Ueda K, Kawamori Y, Gabata T, Kadoya M. Progression to hypervascular hepatocellular carcinoma: Correlation with intranodular blood supply evaluated with CT during intraarterial injection of contrast material. Radiology 2002; 225:143–149.
10. Le Bihan D, Breton E, Lallemand D, Aubin ML, Vignaud J, Laval-Jeantet M. Separation of diffusion and perfusion in intravoxel incoherent motion MR imaging. Radiology 1988; 168:497–505.
11. Le Bihan D, Breton E, Lallemand D, Grenier P, Cabanis E, Laval-Jeantet M. MR imaging of intravoxel incoherent motions: Application to diffusion and perfusion in neurologic disorders. Radiology 1986; 161: 401–407.
12. Turner R, Le Bihan D, Maier J, Vavrek R, Hedges LK, Pekar J. Echo-planar imaging of intravoxel incoherent motion. Radiology 1990; 177: 407–414.
13. Namimoto T, Yamashita Y, Sumi S, Tang Y, Takahashi M. Focal liver masses: Characterization with diffusion-weighted echo-planar MR imaging. Radiology 1997; 204:739–744.
14. Ichikawa T, Haradome H, Hachiya J, Nitatori T, Araki T. Diffusion-weighted MR imaging with a single-shot echoplanar sequence: Detection and characterization of focal hepatic lesions. AJR Am J Roentgenol 1998; 170:397–402.

15. Kim T, Murakami T, Takahashi S, Hori M, Tsuda K, Nakamura H. Diffusion-weighted single-shot echoplanar MR imaging for liver disease. AJR Am J Roentgenol 1999; 173:393–398.
16. Taouli B, Vilgrain V, Dumont E, Daire JL, Fan B, Menu Y. Evaluation of liver diffusion isotropy and characterization of focal hepatic lesions with two single-shot echo-planar MR imaging sequences: Prospective study in 66 patients. Radiology 2003; 226:71–78.
17. Ha WS, Kim CK, Song SH, Kang CB. Study on mechanism of multistep hepatotumorigenesis in rat: Development of hepatotumorigenesis. J Vet Sci 2001; 2:53–58.
18. Fournier LS, Cuenod CA, de Bazelaire C, et al. Early modifications of hepatic perfusion measured by functional CT in a rat model of hepatocellular carcinoma using a blood pool contrast agent. Eur Radiol 2004; 14:2125–2133.
19. Tsuda N, Kato N, Murayama C, Narazaki M, Yokawa T. Potential for differential diagnosis with gadolinium-ethoxybenzyl-diethylenetriamine pentaacetic acid-enhanced magnetic resonance imaging in experimental hepatic tumors. Invest Radiol 2004; 39:80–88.
20. Kojiro M, Roskams T. Early hepatocellular carcinoma and dysplastic nodules. Semin Liver Dis 2005; 25:133–142.
21. Matsui O, Kadoya M, Kameyama T, et al. Benign and malignant nodules in cirrhotic livers: Distinction based on blood supply. Radiology 1991; 178:493–497.
22. Guan S, Zhao WD, Zhou KR, et al. Sequential hemodynamic changes in precancerous lesions of hepatocellular carcinoma: Experimental study with MR perfusion. Chin J Radiol 2006; 40:231–234.
23. Geschwind JF, Artemov D, Abraham S, et al. Chemoembolization of liver tumor in a rabbit model: Assessment of tumor cell death with diffusion-weighted MR imaging and histologic analysis. J Vasc Interv Radiol 2000; 11:1245–1255.
24. Kim YJ, Chang KH, Song IC, et al. Brain abscess and necrotic or cystic brain tumor: Discrimination with signal intensity on diffusion-weighted MR imaging. AJR Am J Roentgenol 1998; 171:1487–1490.
25. Chan JH, Tsui EY, Luk SH, et al. Diffusion-weighted MR imaging of the liver: Distinguishing hepatic abscess from cystic or necrotic tumor. Abdom Imaging 2001; 26:161–165.
26. Lang P, Wendland MF, Saeed M, et al. Osteogenic sarcoma: Noninvasive in vivo assessment of tumor necrosis with diffusion-weighted MR imaging. Radiology 1998; 206:227–235.
27. Deng J, Rhee TK, Sato KT, et al. In vivo diffusion-weighted imaging of liver tumor necrosis in the VX2 rabbit model at 1.5 Tesla. Invest Radiol 2006; 41:410–414.
28. Maier CF, Paran Y, Bendel P, Rutt BK, Degani H. Quantitative diffusion imaging in implanted human breast tumors. Magn Reson Med 1997; 37:576–581.
29. Galons JP, Altbach MI, Paine-Murrieta GD, Taylor CW, Gillies RJ. Early increases in breast tumor xenograft water mobility in response to paclitaxel therapy detected by non-invasive diffusion magnetic resonance imaging. Neoplasia 1999; 1:113–117.